Materials Science

http://www.aimspress.com/journal/Materials/

AIMS Materials Science, 4(4): 867-877.
DOI: 10.3934/matersci.2017.4.867
Received: 30 May 2017
Accepted: 24 July 2017
Published: 01 August 2017

Research article

Electrode–electrolyte interface stability in solid state electrolyte systems: influence of coating thickness under varying residual stresses

Claas Hüter [1,*], Shuo Fu [1,2], Martin Finsterbusch [2], Egbert Figgemeier [3], Luke Wells [3], and Robert Spatschek [1,4]

[1] Institut für Energie- und Klimaforschung IEK-2, Forschungszentrum Jülich, D-52425 Jülich, Germany
[2] Institut für Energie- und Klimaforschung IEK-1, Forschungszentrum Jülich, D-52425 Jülich, Germany
[3] Institut für Stromrichtertechnik und Elektrische Antriebe ISEA, RWTH Aachen University, D-52056 Aachen, Germany
[4] Jülich Aachen Reseach Alliance Energy, RWTH Aachen University, D-52056 Aachen, Germany

[*] **Correspondence:** Email: c.hueter@fz-juelich.de.

Abstract: We introduce a model of electrode–electrolyte interfacial growth which focuses on the effect of thin coating layers on the interfacial stability in prestressed systems. We take into account transport resulting from deposition from the electrolyte, from capillarity driven surface diffusion, and from changes of the chemical potential due to the elastic energy associated with the interface profile. As model system, we use metallic lithium as electrode, LLZO as electrolyte and Al_2O_3 as a thin film interlayer, which is a highly relevant interfacial system in state of the art all-solid-electrolyte batteries. We consider the stability of the electrode-coating-electrolyte interface depending on the thickness of the thin film interlayer and the magnitude of the elastic prestresses. Our central approach is a linear stability analysis based on the mass conservation at the planar interface, employing approximations which are appropriate for solid state electrolytes (SSEs) like LLZ, a thin Li metal electrode and a thin coating layer with a thickness in the range of nanometres.

Keywords: lithium battery; solid state electrolyte; electrode–electrolyte interface; interface stability

1. Introduction

The presented work focuses on the effect of varying interlayer thickness on the stability of the electrode–electrolyte interface, subjected to elastic prestresses. Interfacial stability at the negative electrode (anode) is of specific interest during the recharge phases of batteries, i.e., when the Li^+

ions move from the positive electrode to the negative electrode to get reduced and get deposited. If the Li^+ ions do not deposit uniformly on the electrode, they form protrusions, which can grow as dendrites, one of the main safety-limitations of Li metal batteries. Besides shorting the battery [1, 2, 3], the exothermic reactions at the interface can lead to critical heat production [4, 5], causing further problems.

Besides the improvement by using thermally stable separators, gel electolytes and special additives, the development of solid state electrolytes (SSEs) has proven very fruitful, as current SSEs already exhibit conductivities in the range of 1 mS/cm while providing a much better resistance to dendrite-caused shorting of the cell. Additionally, since all-solid-state batteries (ASBs) can be manufactured using these electrolytes, even in the event of short circuiting via metallic dendrites, a harmful thermal runaway of the cell is intrinsically impossible. However, the SSE–electrode interface exhibits interfacial impedances of about 1000 Ω/cm^2, presenting a major obstacle to the widespread implementation in ASBs due to insufficient power densities. Mitigation strategies against this drawback were explored recently, as experimental work on aluminum oxide coatings in SSEs showed that the interfacial impedance can be drastically reduced [6].

The detailed nature of the suppression of dendrite growth in SSEs was investigated in studies reported in [7, 8, 9]. Here it already was shown that the elastic coefficients of electrode and electrolyte material and residual stresses are of crucial importance. Precisely, if the shear modulus of the electrolyte is at least twice as large as that of the electrode, interface roughening is suppressed, and prestresses at the electrode–electrolyte interface can extend the regime of stability against dendrite formation. Experimental studies reported in [10] support these findings. Due to the interfacial nature of the Li^+ transport and the typical dimensions of Li metal electrodes, the underlying instability we discuss here is related to the formation of islands [11], i.e., it is a short-wavelength instability.

The remaining part of this publication is divided into three sections: a basic overview of the model and the employed approximations, the description of the stability analysis and its outcomes, and the summary.

2. Materials and Method

2.1. Transport Model at the Lithium/Solid Electrolyte Interface

We discuss the processes relevant to the morphological battery stability during the charging half cycle, i.e., when the battery is charged by an applied external current. In general, charge transport in Li-based batteries is governed by electromigration, convection and diffusion across the electrolyte and electrodes. While electromigration describes the motion resulting from the momentum transfer during statistical collisions of electrons and ions [12], convection requires bulk movement of molecules, and diffusion describes an atomistic net motion that follows the opposite gradient of the relevant chemical potential.

However, in the case of solid state electrolytes, these transport processes can be dominated by interfacial transport processes and elastic effects, as here the mechanical response from the electrolyte is pronounced, and the ratio of surface diffusion coefficient to volume diffusion coefficient is orders of magnitude larger than for liquid electrolytes. We assume constant Li^+ concentration in the solid electrolyte, see [13] for a discussion on that issue, which renders the ion flux and electric current proportional to $\nabla\phi$ (ϕ is the electrostatic potential). Assuming Dirichlet boundary conditions at the

electrode–electrolyte interfaces means that the electric potential is linearly dependent on the spatial position. Therefore, we assume the solution of the electric potential ϕ and the interfacial growth at the electrode–electrolyte interface to be decoupled.

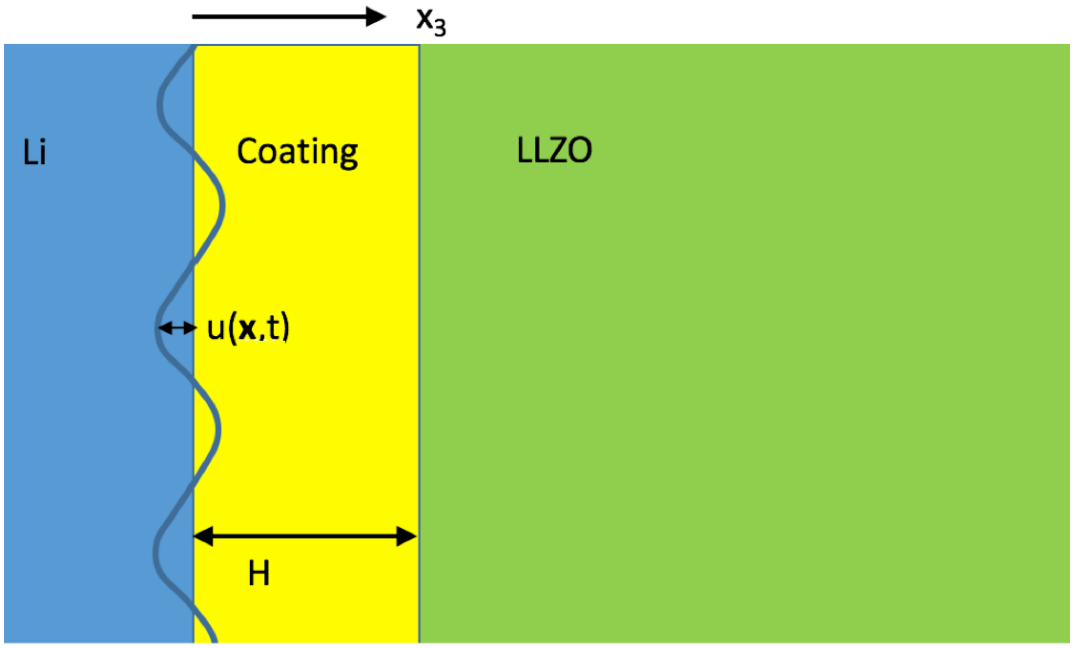

Figure 1. Geometry of the system. The x_3 direction is normal to the planar interfaces, the x_1 and x_2 directions define the plane parallel to the planar interfaces. The protrusion of the interface is denoted as $u(\mathbf{x}, t)$. The interface profile h is moving with an interface velocity along the x_3 axis, υ, as $h(x_1, x_2, t) = \upsilon t + u(\mathbf{x}, t)$. The coating layer of average thickness H connects the solid state electrolyte LLZO and the electrode.

Consequently, we can focus on the Li^+ transport at the interface, and the stability of a protrusion at the planar interface of the thin Li electrode and the solid state electrolyte (SSE). We define the protrusion $h(x_1, x_2, t)$ perpendicular to the plane of the flat electrode/SSE interface, i.e., the Li electrode growing into the SSE, where we neglect the influence of a possible solid-electrolyte-interface (SEI) here as they are less distinctive in LLZ systems. The mass conservation decription associated to the interface profile $h(x_1, x_2, t) = \upsilon t + u(\mathbf{x}, t)$, see Figure 1, follows the extended discussion in [7, 11, 14, 15, 16], and therefore reads as

$$\frac{\partial h}{\partial t} = I - \Omega \nabla \cdot \vec{j}_{surf} + j_\gamma + j_{el} \tag{1}$$

with deposition flux I, partial molar volume of an Li^+ ion solved in the electrolyte Ω, surface flux $\vec{j}_{surf}$, a mass deposition rate j_γ driven by the interfacial energy difference due to the protrusion and a mass deposition rate j_{el} driven by the difference of the elastic energy due to the protrusion. In our model, the deposition flux is governed by the Butler-Volmer equation,

$$i_{Li^+} = i_0 \left(\exp\left(\frac{a_a F}{RT} \eta_s \right) - \exp\left(-\frac{a_c F}{RT} \eta_s \right) \right) \tag{2}$$

where i_{Li^+} is the electric current density, i_0 is the exchange current density which describes the dynamic equilibrium flux density across the interface when anodic and cathodic partial fluxes are equal at zero overpotential. By F we denote the Faraday constant, $a_{a,c}$ are the anodic and cathodic transfer coefficients which we set here as $a_a = a_c = 0.5$, and the overpotential η measures the deviation of the battery system from equilibrium, i.e., $\eta_s = U - V$, where U is the actual potential drop across the electrode/SSE interface and V is the equilibrium potential drop across the electrode/SSE interface. R and T are gas constant and temperature, respectively.

The surface current density relates to classical capillarity-driven surface diffusion and Mullins diffusion, with

$$\vec{j}_{surf} = -\nabla(D_1 h + D_2 \nabla^2 h), \tag{3}$$

$$D_1 = \frac{p_0 \gamma(H/l) \Omega_a^2}{(2\pi M)^{1/2} (k_B T)^{3/2}} \tag{4}$$

$$D_2 = \frac{D_a \gamma(H/l) \Omega_a^2 \nu}{k_B T} \tag{5}$$

with M being atomic weight, Boltzmann constant k_B, equilibrium vapor pressure p_0, atomic number surface density ν, diffusion coefficient D_a (m^2/s), and atomic volume Ω_a. The effective surface energy reads as

$$\gamma(H/l) = \gamma_{LLZO/Al_2O_3} + (\gamma_{Li/LLZO} - \gamma_{LLZO/Al_2O_3})(1 + H/l) \exp(-H/l). \tag{6}$$

It interpolates between the interface energy of the LLZO-Al_2O_3 contact and the interface energy between Li-LLZO, with thickness H of the Al_2O_3 film and l as length scale of about 1 nm, which describes the transition between Al_2O_3 and LLZO. As recently reported in [6], the deposition of thin films, with heights $\sim$ nm, can drastically reduce the surface resistance of the electrode/electrolyte interface and provide better Li growth characteristics.

To estimate the interfacial energy difference $\Delta\gamma = \gamma_{Li/LLZO} - \gamma_{LLZO/Al_2O_3}$, we consider the decohesion energy as upper bound for the interfacial energy, $\gamma_{Li/x} = \gamma_{Li} + \gamma_x - W_{Lix}$. As rough orientation for the work of adhesion W_{Lix} we refer to [17], where first principles calculations for the work of adhesion and self adhesion in Li, Cu as well as Li and Cu oxides were reported. We assume a constant ratio of surface energy per nearest neighbour distance and bulk modulus [18], $\gamma/(Ba) \sim \beta$, where $\beta \approx 0.03$ is a typical value for the ratio of surface energy per lattice distance and bulk modulus. As average for the nearest neighbour distance, we choose $a \approx 0.21$ nm for Al_2O_3, $a \approx 0.23$ nm for cubic LLZO, and $a \approx 0.27$ nm for Li. With $B_{LLZO} \approx 100$ GPa, $B_{Al_2O_3} \approx 150$ GPa and $B_{Li} \approx 10$ GPa, we estimate $\Delta\gamma \approx 0.6$ J/m^2. For the exchange current i_0, we assume that the thickness of the Al-oxide layer is always sufficient to reduce the impedance owed to the geometric mismatch of the SSE grains and the Li foil, providing approximately a constant exchange current density for varying heights of the Al oxide layer.

The mass deposition rate relating to the interfacial energy difference due to the protrusion reads as

$$j_\gamma = -\frac{\Omega K d}{RT} \frac{\delta}{\delta h} \int_A \frac{\gamma(H/l)}{2} |\nabla h|^2 d\vec{x}, \tag{7}$$

with interfacial area A, and the mass deposition rate related to the elastic energy density f^{el} reads as [7],

$$j_{el} = -\frac{\Omega K d}{RT}\frac{\delta}{\delta h}\int_A f^{el}[\sigma^*_{ij}, h]d\vec{x}. \tag{8}$$

For the equilibrium exchange rate coefficient it holds $K = i_0\Omega/(dF)$, with atomic interplanar distance d in the electrode. We assume that the Li/SSE interface is subjected to stress discontinuities tangential to the interface caused by pressure applied during single cell manufacturing, serial stacking, etc., and the difference in the elastic parameters of the electrode and the electrolyte. Therefore, we consider the elastic problem independent of the coating layer thickness, focusing on the Li–LLZO interface for the solution of the elastic problem. The resulting mass conservation then yields

$$\frac{\partial h}{\partial t} = \frac{Kd}{RT}z_+F\eta + \nabla^2(D_1h + D_2\nabla^2 h) - \frac{\Omega K d}{RT}\gamma\nabla^2 h - \frac{\Omega K d}{RT}\frac{\delta}{\delta h}\int_A f^{el}[\sigma^*_{ij}, h]d\vec{x}, \tag{9}$$

where we linearised the deposition contribution described by the Butler-Volmer equation for small current densities, $i_{Li^+}/i_0 \ll 1$, and focus from now on the influence of the ratio of film thickness and characteristic length scale of the interface, H/l.

3. Results and Discussion

3.1. Linear Stability Analysis: Effect of Thin Films at the Electrode–Electrolyte Interface

When we introduce the perturbation ansatz as

$$h(x_1, x_2, t) = \upsilon t - u(x_1, x_2, t). \tag{10}$$

$$u(x_1, x_2, t) = Ae^{-\lambda t}e^{-i\vec{k}\cdot\vec{x}}, \tag{11}$$

we locate the origin of the coordinate system at the interface steadily moving at velocity $\upsilon = Kdz_+F\eta_s/RT$. Therefore, the constant deposition flux is eliminated from the mass conservation, and with the explicit representation of the surface fluxes, we consider the influence of the Al oxide film thickness on the stability of the electrode–eletrolyte interface in terms of

$$\frac{\partial h}{\partial t} = (D_1 + D_3)\nabla^2 h + D_2\nabla^4 h, \tag{12}$$

skipping the elastic contributions first. For the coefficients $D_{1,3}$, it holds $D_1 \ll D_3$ with the additionally defined diffusion coefficient $D_3 = \Omega K d\gamma(H/l)/RT$. For a convenient presentation of the Al oxide layer thickness dependence, we express Eq. (12) as

$$\frac{\partial h}{\partial t} = D_3^0\left(a + (1-a)\left(1 + \frac{H}{l}\right)e^{-\frac{H}{l}}\right)\nabla^2 h + D_2^0\left(a + (1-a)\left(1 + \frac{H}{l}\right)e^{-\frac{H}{l}}\right)\nabla^4 h, \tag{13}$$

where $D_2^0 = D_s\gamma_{Li/LLZO}\Omega_m^2\nu/k_BT$, $D_3^0 = \Omega K d\gamma_{Li/LLZO}/RT$ and $a = \gamma_{LLZO/Al_2O_3}/\gamma_{Li/LLZO}$. For the interfacial contribution $\sim \gamma(H/l)\nabla^2 h$, we assume that the height of the Li layer H will be much larger than the magnitude of the protrusion h, i.e., $h/H \ll 1$, which lets us neglect the dependence of the interfacial energy on the protrusion and simplifies the analytical treatment. Therefore, we note that the

stability analysis requires a sufficient thickness of the aluminum oxide film. The resulting equation for the stability parameter λ becomes

$$\lambda = D_3^0\left(a+(1-a)\left(1+\frac{H}{l}\right)e^{-\frac{H}{l}}\right)|k|^2 - D_2^0\left(a+(1-a)\left(1+\frac{H}{l}\right)e^{-\frac{H}{l}}\right)|k|^4, \tag{14}$$

$$\lambda = \frac{\lambda^0}{\left(a+(1-a)\left(1+\frac{H}{l}\right)e^{-\frac{H}{l}}\right)}, \tag{15}$$

with the wavelength λ^0 that corresponds zero thickness of the aluminium oxide film, $\lambda^0 = \lambda(H/l = 0)$. Apparently, for the prediction of the critical wavelength k_c where $\lambda = 0$, the influence of the aluminum oxide layer thickness vanishes, as $k_c \sim \sqrt{D_3/D_2}$. The reduced growth factor in the unstable regime means that with increasing coating thickness, the growth velocity of the protrusion is exponentially reduced, see Figure 2, though the instability cannot be fully prevented.

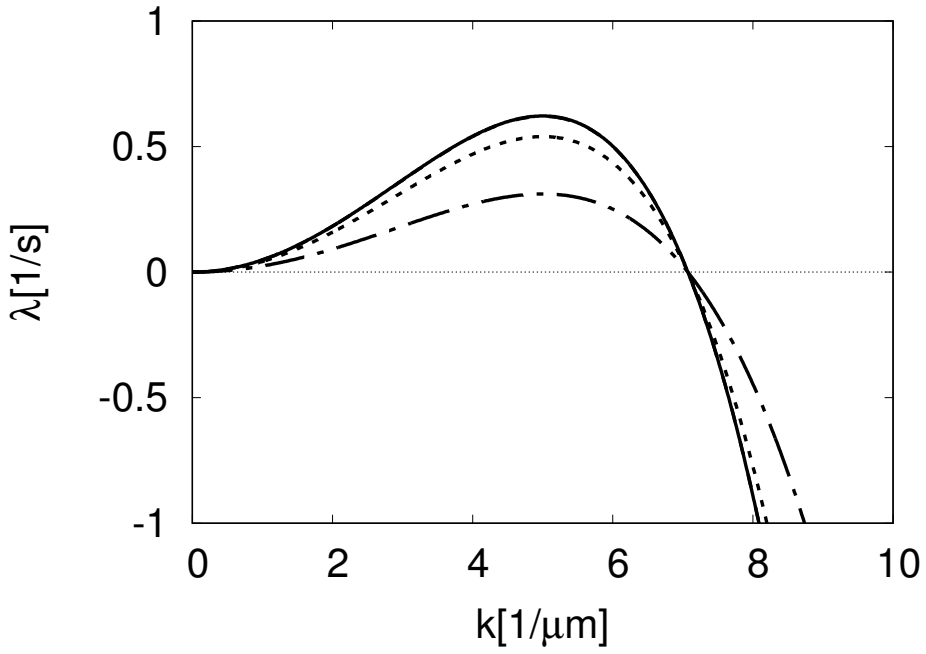

Figure 2. Growth parameter λ [s^{-1}] vs wave vector k [μm^{-1}]. The bold solid curve corresponds to a ratio of coating thickness to characteristic lengthscale $H/l = 0.0$, the curve for $H/l = 0.1$ nearly coincides with the curve for $H/l = 0.0$, the dashed curve corresponds to a ratio of coating thickness to characteristic lengthscale $H/l = 1$ and the dashed-dotted curve corresponds to a ratio of coating thickness to characteristic lengthscale $H/l = 10$. While the coating thickness does not shift the critical wavelength, increasing coating thicknesses provide exponentially slower growth in the unstable regime $k > k_c$.

By introducing the elastic contribution coming from the prestresses, we can expect an effect of the layer thickness on the critical wavelength. Therefore, we introduce the elastic problem at the interface next, following the analysis of the stabiltity of a nearly flat interface described in [19, 20].

3.2. Linear Stability Analysis: Influence of Prestresses and Coating Film Thickness

For the description of the elastic model of the electrolyte–electrode interface, we stay in the regime of linear elasticity and consider the initially flat interface which is subject to a prestress as it results from cell manufacturing and stacking of the battery cells, independent of the coating thickness. Taking into account that the bulk moduli of Li and LLZO or Al_2O_3 differ by an order of magnitude, restricting the elastic contribution to the Li–Al_2O_3 interface is suggested. As the lattice constants for Li and Al_2O_3 are very close, we neglect here also possible coherency stress contributions. This decoupling allows us to provide an analytically tractable estimate of the stability of the interface.

We introduce the residual stress field $\sigma_{ij}^{(p,E/S)}$ in the solid (S) or electrolyte (E) that is associated to a prestrain field $\epsilon_{ij}^{(p,E/S)}$, which is equilibrated at a flat interface,

$$\epsilon_{ij}^{p} = \epsilon_{ij}^{p,E} | x_3 > 0, \tag{16}$$

$$\epsilon_{ij}^{p} = \epsilon_{ij}^{p,S} | x_3 < 0, \tag{17}$$

$$\sigma_{ij} = -c_{ijkl}^{E} \epsilon_{kl}^{p,E} = \sigma_{ij}^{p,E} | x_3 > 0, \tag{18}$$

$$\sigma_{ij} = -c_{ijkl}^{S} \epsilon_{kl}^{p,S} = \sigma_{ij}^{p,S} | x_3 < 0, \tag{19}$$

$$\sigma_{i3}^{p,E} - \sigma_{i3}^{p,S} = 0 | x_3 = 0, \tag{20}$$

$$\sigma_{i3}^{E} - \sigma_{i3}^{S} = t_i, \tag{21}$$

$$\vec{u}^{E} = \vec{u}^{S} | x_3 = 0, \tag{22}$$

$$u_i \to 0 | x_3 \to \pm\infty. \tag{23}$$

Assuming a serial stacking of the cells with pressure σ_{33}^{stack} perpendicular to the interface, the resulting biaxial discontinuities of the equilibrated prestress tangential components across the interface, read as

$$\Delta\sigma^{p} = \sigma_{ij}^{p,E} - \sigma_{ij}^{p,S}, \tag{24}$$

$$\Delta\sigma_{11,22}^{p} = \left(\frac{c_{12}^{E}}{c_{11}^{E}} - \frac{c_{12}^{S}}{c_{11}^{S}} \right) \sigma_{33}^{stack}, \tag{25}$$

$$t_i = \Delta\sigma_{ij}^{p} n_k, \tag{26}$$

where we refer to the work of Mikhaylik et al. [10] on a lithium anode/dioxolane-dimethoxyethane (DOL + DME) system for the values of the elastic coefficients $c_{ij}^{E/S}$.

When we introduce the interface protrusion, the difference in the elastic energy of the perturbed system and the flat interface system can conveniently be expressed in terms of the tractions associated to the protrusion. We follow the approach described in [7], thus corrections of the electrical field and the concentration field vanish to first order. We define a correction displacement field $\vec{u}$, which introduces terms proportional to $|\nabla h|$ in leading order and satisfies

$$\frac{\partial \epsilon_{ij}^{E}(u)}{\partial x_j} = 0 | x_3 < h(x_1, x_2, t), \tag{27}$$

$$\frac{\partial \epsilon_{ij}^{S}(u)}{\partial x_j} = 0 | x_3 > h(x_1, x_2, t), \tag{28}$$

$$\sigma^E_{i3}(u) - \left(\sigma^{p,E}_{i\beta} + \sigma^E(u)_{i\beta}\right)\frac{\partial h}{\partial x_\beta} = \tag{29}$$

$$\sigma^S_{i3}(u) - \left(\sigma^{p,S}_{i\beta} + \sigma^S(u)_{i\beta}\right)\frac{\partial h}{\partial x_\beta}|z = h(x_1, x_2, t),$$

$$u_i \to 0|z \to \pm\infty, \tag{30}$$

$$\sigma^S_{ij}(u) = c^S_{ijkl}\varepsilon^S_{kl}(u), \tag{31}$$

$$\sigma^E_{ij}(u) = c^E_{ijkl}\varepsilon^E_{kl}(u). \tag{32}$$

Defining this displacement relative to the protrusion, $u_i(x_1, x_2, x_3, t) = v_i(x_1, x_2, x_3 - h(x_1, x_2, t), t)$, the resulting representation of the equilbirium problems reads as

$$\frac{\partial \sigma^E_{ij}}{\partial x_j}(v) = 0|x_3 > 0, \tag{33}$$

$$\frac{\partial \sigma^S_{ij}}{\partial x_j}(v) = 0|x_3 < 0, \tag{34}$$

$$\sigma^E_{i3}(v) - \sigma_{i\beta^{p,E}}\frac{\partial h}{\partial x_\beta} = \sigma^S_{i3}(v) - \sigma^{p,S}_{i\beta}\frac{\partial h}{\partial x_\beta}|x_3 = 0, \tag{35}$$

$$v_i \to 0|x_3 \to \pm\infty, \tag{36}$$

and the difference of the elastic energy due to the perturbed interface is obtained as

$$\Delta E^{el} = \int_{\mathbb{R}^2}\int_{\mathbb{R}^2}\frac{1}{2}G_{ik}(\vec{x} - \vec{x}')\Delta\sigma^p_{i\beta}\Delta\sigma^p_{k\delta}\frac{\partial h}{\partial x_\beta}\frac{\partial h}{\partial x'_\delta}d\vec{x}d\vec{x}'. \tag{37}$$

For the numeric evaluation of the interface Greens tensor, we implemented the approach described in [7], based on the representation of the elastic problem in terms of Fourier transforms. Using available elastic parameters of LLZO [21] and Li, it reduces the determination of the Greens tensor for LLZO to the solution of a quadratic eigenvalue problem. It provides the Fourier Transform $\hat{G}_{ik}$, which relates to the Greens tensor as

$$\int_{-\infty}^{\infty}\int_{-\infty}^{\infty}\frac{1}{2}\hat{G}_{ik}\hat{t}_i(k_1, k_2)\hat{t}^p_k(k_1, k_2)dk_1dk_2 = \int_{\mathbb{R}^2}\int_{\mathbb{R}^2}G_{ik}(\vec{x} - \vec{x}')t_i(\vec{x})t_k(\vec{x}')d\vec{x}d\vec{x}', \tag{38}$$

with $\hat{t}^p_i$ being the Fourier transform of the traction t^p_i due to the prestresses. We employ octave, an open-source mathematical programming language [22], which provides a polynomial order eigenvalue problem solver. The elastic contribution is of main interest for biaxial tangential stress discontinuities caused by a stacking pressure as described in Eq. (24). Here it is

$$\hat{G}_{ik}\Delta\sigma^p_{i\beta}\Delta\sigma^p_{k\delta}k_\delta k_\delta = \left(\hat{G}_{11}\Delta{\sigma^p_{11}}^2 + \hat{G}_{12}\Delta\sigma^p_{11}\Delta\sigma^p_{22} + \hat{G}_{21}\Delta\sigma^p_{22}\Delta\sigma^p_{11} + \hat{G}_{22}\Delta{\sigma^p_{22}}^2\right). \tag{39}$$

The resulting representation of the flux due to the elastic energy of the pertrubed interface in Eq. (9) thus reads as

$$j_{el} = -\frac{Kd}{RT}\int_{R^2}\frac{\partial G_{ik}}{\partial x_\beta}(\vec{x} - \vec{x}')\Delta\sigma^p_{i\beta}\Delta\sigma^p_{k\delta}\frac{\partial h}{\partial x'_\delta}d\vec{x}', \tag{40}$$

which leads to the stability consideration for prestressed electrode-electrolyte interfaces at varying thicknesses.

As we take the influence of the prestresses at the perturbed interface into account, Eq. (14) is extended to

$$\lambda = D_3^0\left(a + (1-a)\left(1+\frac{H}{l}\right)e^{-\frac{H}{l}}\right)|k|^2 - D_2^0\left(a + (1-a)\left(1+\frac{H}{l}\right)e^{-\frac{H}{l}}\right)|k|^4 + D_4\hat{G}_{ik}\Delta\sigma^p_{i\beta}\Delta\sigma^p_{k\delta}k_\delta k_\delta. \quad (41)$$

We note that $\hat{G}_{ik}$ is positive, therefore the elastic contribution always provides a stabilizing influence. To perform the linear stability analysis, we used values and the approximations we already employed in the previous stability analysis, taken from [6, 7, 10, 17, 18]. The resulting plot in Figure 3 shows that while the effect of the thickness of the interface in absence of elastic effects does not shift the critical wavelength k_c, it leads to an additional shift of k_c when the interface is stabilized due to prestresses.

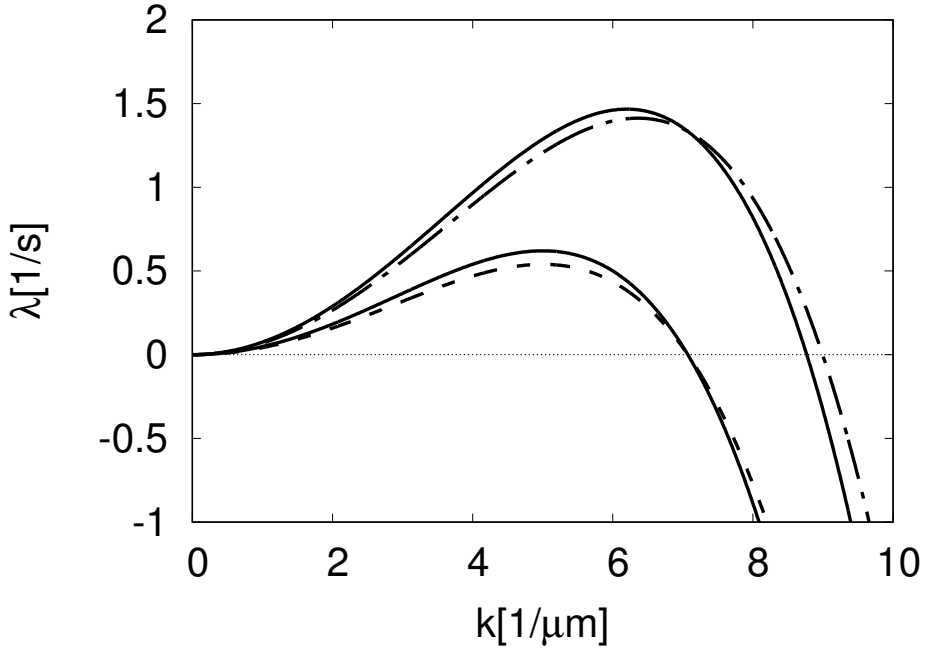

Figure 3. Growth parameter λ [s^{-1}] vs wave vector k [μm^{-1}], the upper solid line corresponds to prestresses of 500 MPa and a ratio of interfacial thickness to characteristic lengthscale H/l = 0.1, the lower solid line corresponds to zero prestresses and a ratio of interfacial thickness to characteristic lengthscale H/l = 0.1, the dashed-dotted line corresponds to prestresses of 500 MPa and a ratio of interfacial thickness to characteristic lengthscale H/l = 1, the dashed line corresponds to zero prestresses and a ratio of interfacial thickness to characteristic lengthscale H/l = 1.

4. Conclusions

We considered the effect of a thin interlayer between the SSE and the Li-metal electrode on the stability of electrode-electrolyte interfaces depending on the presence of an elastic prestress and the thickness of the interlayer. By means of a linear stability analysis, the influence of the interlayer is

found to be beneficial, implying a reduced growth velocity in the unstable regime and an extension of the stable growth regime when also residual stresses are present as well. We used material parameters for metallic Li, Al_2O_3 and LLZO or approximations thereof to quantify these effects. The positive influence of the interlayer and residual stresses suggests a more detailed analysis which then should take possible coherency stresses at the electrode-interlayer interface in addition to the residual stresses into account, and provides a discussion of the nonlinear feedback of the interface protrusion in the regime of developed dendrite growth. These considerations require a comprehensive nonlinear stability analysis which also includes the corrections in the electric potential and the Li^+ concentration. Since dendrite prevention is a topic of major importance in ASB research, this will be pursued in the future.

Acknowledgments

This work is funded by the BMBF project Meet HiEnd II.

Conflict of Interest

All authors declare no conflict of interest in this paper.

References

1. Bhattacharayya R, Key B, Chen H, et al. (2010) In situ observation NMR observation of the formation of metallic lithium microstructures in lithium batteries. *Nat Mater* 9: 504.
2. Chandrashekar S, Trease NM, Chang HJ, et al. (2012) ^{7}Li MRI of Li batteries reveals location of microstructural lithium. *Nat Mater* 11: 311.
3. Harry KJ, Hallinan DT, Parkinson DY, et al. (2014) Detection of the subsurface structures underneath dendrites formed on cycled lithium metal electrodes. *Nat Mater* 13: 69.
4. von Sacken U, Nodwell E, Sundher A, et al. (1995) Comparative thermal stability of carbon intercalation anodes and lithium metal anodes for rechargable lithium batteries. *J Power Sources* 54: 240.
5. Tobishima SI, Yamaki JI (1999) A consideration of lithium cell safety. *J Power Sources* 81: 882.
6. Han X, Gong Y, Fu K, et al. (2017) Negating interfacial impedance in garnet-based solid-state Li metal batteries. *Nat Mater* 16: 572.
7. Natsiavas PP, Weinberg K, Rosato D, et al. (2016) Effect of prestress on the stability of electrode–electrolyte interfaces during charging in lithium batteries. *J Mech Phys Solids* 95: 92–111.
8. Ely DR, Garcia RE (2013) Heterogeneous nucleation and growth of lithium electrodeposits on negative electrodes. *J Electrochem Soc* 160: A662–A668.
9. Nishida T, Nishikawa K, Rosso M, et al. (2013) Optical observation of Li dendrite growth in ionic liquid. *Electrochim Acta* 100: 333–341.
10. Mikhaylik YV, Kovalev I, Schock R, et al. (2010) High energy rechargable Li-S cells for EV application: status, remaining problems and solutions. *ECS Trans* 25: 23–34.

11. Ortiz M, Repetto EA, Si H (1999) A continuum model of kinetic roughening and coarsening in thin films. *J Mech Phys Solids* 47: 697.
12. Ho PS, Kwok T (1989) Electromigration in metals. *Rep Prog Phys* 52: 301.
13. Newman J, Thomas-Alyea KE (2012) *Electrochemical Systems*, Hoboken, New Jersey, USA: John Wiley and Sons.
14. Mullins WW (1957) Theory of thermal grooving. *J Appl Phys* 28: 333–339.
15. Herring C (1951) Surface tension as a motivation for sintering, *The Physics of powder metallurgy*, New York: McGraw-Hill.
16. Das Sarma S, Ghaisas SV (1992) Solid-on-solid rules and models for nonequilibrium growth in 2 + 1 dimensions. *Phys Rev Lett* 69: 3762.
17. Martin L, Vallverdu G, Martinez H, et al. (2012) First principles calculations of solid–solid interfaces: application to conversion materials for lithium-ion batteries. *J Mater Chem* 22: 22063.
18. Weir G (2008) Implications from the ratio of surface tension to bulk modulus and nearest neighbour distance, for planar surfaces. *Proc R Soc A* 464: 2281.
19. Srolovitz D (1989) On the stability of surfaces of stressed solids. *Acta Metall* 37: 621.
20. Gao H (1991) Stress Concentration at slightly undulating interfaces. *J Mech Phys Solids* 39: 443.
21. Yu S, Schmidt RD, Garcia-Mendez R, et al. (2016) Elastic Properties of the Solid Electrolyte $Li_7La_3Zr_2O_{12}$(LLZO). *Chem Mater* 28: 197.
22. Murphy M (1997) Octave: A Free, High-Level Language for Mathematics. *Linux J* 39: 1225.

AIMS Press